Using Geophysical Methods to Study the Shallow Subsurface of a Sensitive Alpine Environment, Niwot Ridge, Colorado Front Range, U.S.A

Authors: Leopold, Matthias, Dethier, David, Völkel, Jörg, Raab, Thomas, Rikert, Tyler Corson, et al.

Source: Arctic, Antarctic, and Alpine Research, 40(3) : 519-530

Published By: Institute of Arctic and Alpine Research (INSTAAR), University of Colorado

URL: https://doi.org/10.1657/1523-0430(06-124)[LEOPOLD]2.0.CO;2

Arctic, Antarctic, and Alpine Research, Vol. 40, No. 3, 2008, pp. 519–530

Using Geophysical Methods to Study the Shallow Subsurface of a Sensitive Alpine Environment, Niwot Ridge, Colorado Front Range, U.S.A.

*Matthias Leopold**
David Dethier†
Jörg Völkel‡
Thomas Raab§
Tyler Corson Rikert† and
Nel Caine#

*Corresponding author:
Geomorphology and Soil Science, Research Department of Ecology and Ecosystem Sciences, Center of Life and Food Sciences Weihenstephan, Technische Universität München, 85354 Germany
leopold@wzw.tum.de
†Department of Geosciences, Williams College, Williamstown, Massachusetts 01267, U.S.A.
‡Geomorphology and Soil Science, Research Department of Ecology and Ecosystem Sciences, Center of Life and Food Sciences Weihenstephan, Technische Universität München, 85354 Germany
§Chair of Soil Protection and Recultivation, Faculty of Environmental Science and Process Engineering, BTU Cottbus, 03013 Germany
#Department of Geography, University of Colorado at Boulder, Boulder, Colorado 80309, U.S.A.

Abstract

Shallow seismic refraction (SSR) and ground penetrating radar (GPR) are non-invasive geophysical techniques that enhance studies of the shallow subsurface deposits which control many geomorphic and biogeochemical processes. These techniques permit measuring the thickness and material properties of these deposits in sensitive alpine areas without using extensive pits and trenches that can impact current biogeospheric processes or distort them for future research. Application of GPR and SSR along 1.5 km of geophysical lines shows that layers of fine to coarse, blocky deposits of periglacial origin underlie alpine slopes in the vicinity of Niwot Ridge, Colorado Front Range. Interpretation of geophysical and drilling data shows that depth to bedrock ranges from 4 to >10 m and is not simply related to local slope. Our measurements suggest that ice lenses form seasonally beneath solifluction lobes; ice was not present in adjacent areas. Ice lenses are associated with local ponded water and saturated sediments that result from topographic focusing and low-permeability layers beneath active periglacial features. Geophysical interpretations are mainly consistent with data derived from nearby drill cores and corroborate the utility of GPR in combination with SSR for collecting subsurface data required by different landscape models in sensitive alpine environments.

DOI: 10.1657/1523-0430(06-124)[LEOPOLD]2.0.CO;2

Introduction

Non-invasive geophysical techniques such as shallow seismic refraction (SSR) and ground penetrating radar (GPR) permit detailed investigation of the shallow subsurface, which we use here for the organic and inorganic material that rests on unweathered bedrock.

The shallow subsurface has become a major focus for geoscience research in the United States and is called in a summarized way the critical zone. "The Critical Zone can be considered a reactor supplied with unweathered rock through uplift and erosion, fluids through precipitation, and stirred at the top by biological and physical processes" (Anderson et al., 2007, p. 315).

The texture and layering of the critical zone reflects and controls geomorphic processes as well as many processes that influence the adjacent biogeosphere; e.g. soil hydrology, nutrient and gas flux, temperature regime, and pedogenesis. In dissected upland landscapes such as those of the Colorado Front Range, the critical zone is composed of slope deposits of varying genesis, thickness, age, composition, and 3-D shape. Weathering and soil-forming processes, periglacial activity, soil creep, and other mass movements slowly alter and mix the subsurface to form a more or less complex sequence of strata (e.g. Hambrey, 1994; Menzies, 1996; Kleber, 1997; Benn and Evans, 1998; Völkel et al., 2001; Birkeland et al., 2003; Raab and Völkel, 2003; Leopold and Völkel, 2007a; Raab et al., 2007). In long term settlement areas like Europe, human-induced erosion processes are also a major factor in the transformation of the strata (Leopold and Völkel, 2007b). Analysis of these strata is especially important for ecologically oriented models (Seastedt et al., 2004). The base of the shallow subsurface, the contact zone of weathered material and the upper meters of bedrock, represents an important hydrogeochemical transition in many environments.

Collecting representative data from the critical zone produces three basic challenges. First, natural or excavated sections like gullies, pits, and borings are labor-intensive, spatially limited, and logistically challenging in remote areas (e.g. using an excavator). Second, despite careful study, experience, and the best of intentions, it is usually hard to predict what an excavation will expose. Finally, most excavations necessarily alter the layering and hydrologic properties of the shallow subsurface, potentially

1523-0430/08 $7.00

impacting both nearby and future measurements. Minimizing the impact of subsurface studies is particularly crucial in climate-sensitive ecosystems such as alpine zones (Leopold et al., 2006).

In this paper we briefly describe the application of SSR and GPR to the shallow subsurface, and report initial results from research in the vicinity of the long term ecological research site (LTER) on Niwot Ridge, Colorado Front Range, U.S.A. The two techniques produce negligible site impact, allow careful targeting of necessary excavations and, in conjunction with other measurements, produce 2-D models of the critical zone.

AN INTRODUCTION TO SHALLOW SEISMIC REFRACTION AND GROUND PENETRATING RADAR

Shallow seismic refraction (SSR) techniques use the principle that seismic (acoustic) waves travel with different velocities in materials of different density, which led to initial seismic imaging methods in the late 19th and early 20th centuries. Because the subsurface consists of different materials with different densities (e.g. soil parent material, regolith, bedrock), layer thickness and contact relations can be measured where conditions are favorable. Seismic refraction is especially suitable for detecting the contact between regolith and bedrock, as these materials have distinct acoustic wave travel times (see Burger et al., 2006). Depending on the energy source (e.g. sledgehammer), possible penetration is at least some tens of meters. Resolution of single layers depends mainly on thickness and density differences and geophone spacing. The method requires increasing density of material with depth, and acoustic wave penetration is reduced by air between boulders that are common in alpine areas. Where subsurface layers change over short distances to materials of sharply different density (e.g. boulders without fines to small rock fragments with abundant fines), resulting "hidden layers" or other artifacts make interpretation challenging (Burger et al., 2006). In these cases additional data from boreholes or nearby natural exposures helps with the interpretation.

In contrast to SSR, GPR uses electromagnetic (EM) energy to survey the shallow subsurface. EM waves at frequencies from 10 MHz to over 1.5 GHz are radiated into the ground and are reflected based on different dielectric properties of subsurface materials. Reflected waves are received back at the surface according to a general principle: the higher the frequency, the better the resolution and the shallower the penetration depth (Jol and Bristow, 2003). The depth of penetration ranges from a few decimeters to several meters at high frequency (>500 MHz) and up to decameters for low frequency (<200 MHz) antennae. Water strongly influences the theoretical resolution limit, which is ¼ to ½ of the wavelength (Sheriff and Geldart, 1982). For example, at 100 MHz, theoretical resolution in a saturated sand is 0.15 to 0.3 m and 0.375 to 0.75 m in a dry sand (Jol and Bristow, 2003). Better resolution in saturated materials often results in less penetration because sedimentary heterogeneity and high water content together with silt and clay-rich sediments attenuate the signal and reduce the wave velocity (Moorman et al., 2003). Therefore, antennae frequency must reflect the requirements of a specific survey (Neal, 2004). In alpine zones, boulders can cause diffraction signals. Active and fossil periglacial slope deposits, rock glaciers, and other periglacial forms have been successfully characterized using GPR by several authors (e.g. Völkel et al., 2001; Sass and Wollny, 2001; Berthling et al., 2003; Degenhardt et al., 2003; Leopold and Völkel, 2003; Otto and Sass, 2006; Munroe et al., 2007). SSR measurements allow a survey sufficiently deep to portray the bedrock contact and to give information about a basic layering. GPR measurements can give a detailed image of the upper meters of the subsurface (Neal, 2004). Subsurface information derived from the two different methods can be used for a combining geomorphic interpretation.

Setting

The sites studied on Niwot Ridge (Fig. 1a) consist of upland surfaces and adjoining slopes near the crest of the Colorado Front Range on the eastern flank of the Rocky Mountains. The range slopes from elevations over 4000 m a.s.l. down to the Colorado Piedmont and High Plains at 1500 m with correspondingly strong temperature and moisture contrasts that control altitudinal zonation of vegetation and soil types (Barry, 1973; Birkeland et al., 2003). The study sites are located in the alpine tundra zone above the late Pleistocene ice limit (Gable and Madole, 1976); mean annual temperature at 3743 m is −3.7°C and annual precipitation is about 930 mm (Greenland, 1989). The Niwot Ridge area is a LTER-site managed by the University of Colorado in cooperation with the U.S. Forest Service and includes the 1200 ha Niwot Ridge Biosphere Reserve, a site for research and education.

Geomorphic, hydrologic, climatic, and biogeochemical aspects of the Niwot Ridge area have been studied in considerable detail over the past 50 years, including pioneering work on periglacial landforms (Benedict, 1970), processes, and rates of transport (cf., http://www.colorado.edu/mrs/mrspubs.html). Despite such extensive studies, the shallow subsurface in the Niwot Ridge area is not well characterized. Numerous short, shallow trenches, soil pits, and auger holes provide a wealth of local information, but we are aware of only one study that investigated deposits over a horizontal distance of more than 10 m (Madole, 1982).

From 20 to 27 July 2005, we collected SSR lines near Martinelli Snowfield at 3440 m (Fig. 1b) and on Niwot Ridge at a site informally called Niwot Trough at 3440 to 3410 m (Fig. 1c), and GPR lines at the East Knoll (3535 m) and at the "Fahey site" at 3500 m (Ives and Fahey, 1971; see Fig. 1d), the location of doctoral studies by B. D. Fahey. The lower part of the Fahey site was investigated in detail by Benedict (1970) in his landmark study of periglacial processes. He mapped numerous turf-banked lobes and terraces in the vicinity of the Fahey site and carefully monitored a turf-banked lobe (his site 45) some 50 m downslope (Benedict, 1970). After our field studies were completed, a series of auger holes (borings) were made in mid-September for the University of Colorado adjacent to the geophysical lines at Martinelli and at the Fahey site, providing us with basic stratigraphic information useful in calibrating our geophysical models at these sites.

Methods

FIELD DESCRIPTION

We surveyed the topography of the geophysical lines using tape, compass and inclinometer and collected a detailed description of each line during SSR or GPR surveys, noting surface rock sizes, areas with or without vegetation cover, and the areas of water and discontinuous surface drainage that form seasonally on these slopes. We located line positions using GPS.

BORINGS

After the geophysical studies were completed, holes for groundwater wells and other instrumentations were drilled in mid-

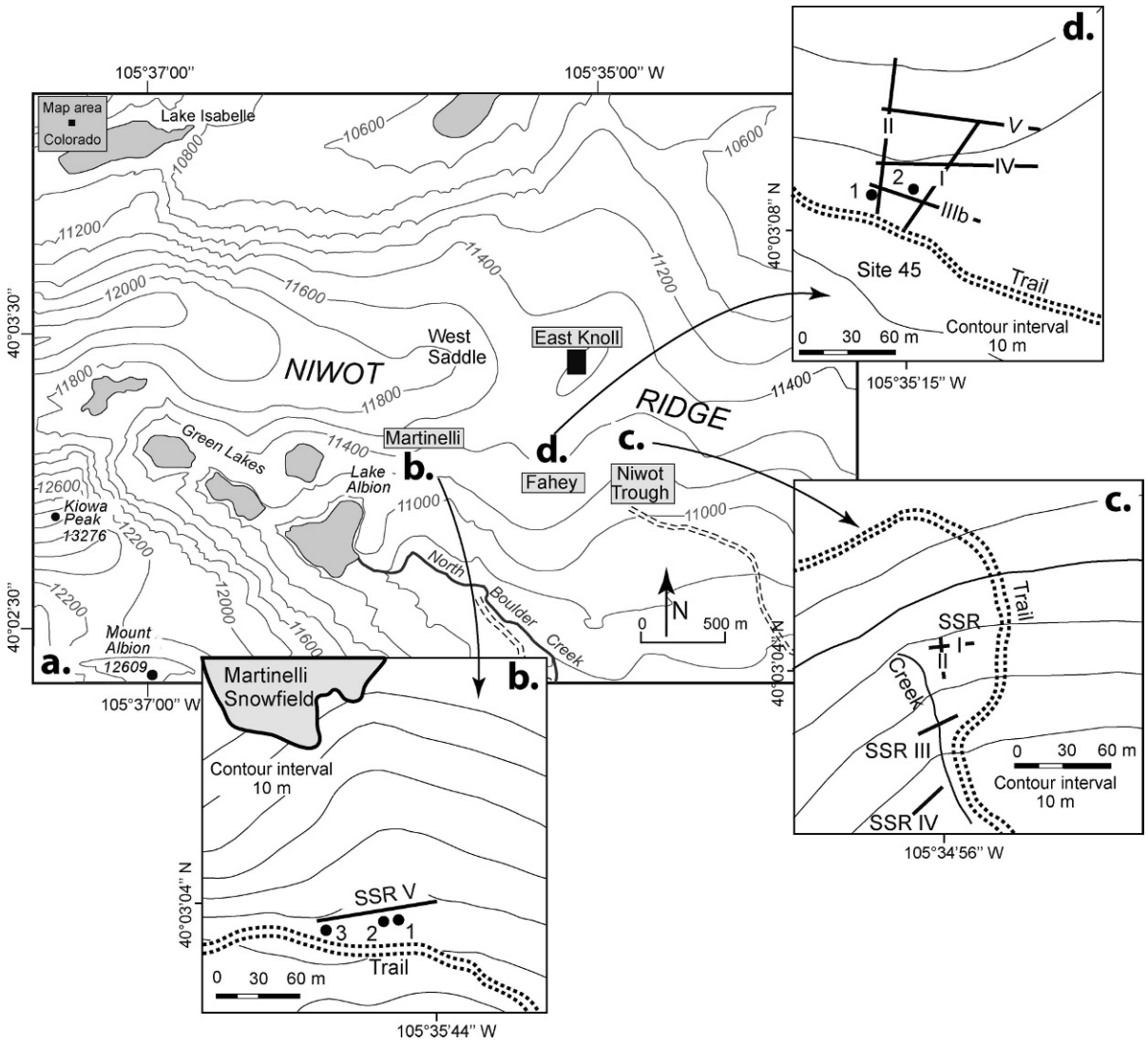

FIGURE 1. (a) Map of the Niwot Ridge area and insets of the study sites "Martinelli Snowfield" (b), "Niwot Trough" (c), and "Fahey" (d). Map base for contour lines (ft), lakes, and peaks is the Ward (1978) 7.5′ Quadrangle. Inset of Martinelli Snowfield (b) shows seismic refraction line SSR V and numbered bullets indicate the location of borings adjacent to the line and north of the trail to the Green Lakes. Inset of Niwot Trough (c) shows location of four seismic refraction lines Niwot SSR I–IV beside the trail to Niwot Ridge. Inset of Fahey site (d) north of the trail to the Tundra Laboratory at Niwot Ridge shows GPR lines I–V; bullets numbered 1 and 2 indicate the location of borings.

September using an air compressor boring technique. Beside low costs, this light-weight technique has minimal impact on the surface, which is important to minimize environmental damage at the LTER–site at Niwot Ridge. However, because this technique disaggregates subsurface material and blows it out of the hole, precise subsurface field description is difficult. Thus there is no core to examine and reconstruction of the lithogenic structure is based on the speed of movement of the drill rig (e.g. slower through more competent rock) and the type of material brought to the surface (e.g. solid rock fragments, wet material, organic rich). Therefore, we mainly use the description from the drillings (1) for estimating depth to bedrock, (2) to distinguish between wet and dry strata, (3) to approximate the content of organic material due to the change of color, and (4) for rough estimation of the content of finer material (e.g. the sand to clay-size fractions). Boreholes #1 to #3 at the Martinelli site were located within 10 m of the line to the north and south. At the Fahey site, Borehole #1 was on the solifluction lobe, whereas #2 was at the edge of the solifluction lobe described in the text.

SHALLOW SEISMIC REFRACTION (SSR) AND GROUND PENETRATING RADAR (GPR)

We used a 12-channel seismic system, Smartseis (Geometrics), for SSR with a geophone spacing of 3 m and 7 m, resulting in line lengths of 33 m or 91 m. An iron sledgehammer (~5 kg) served as an energy source with an electronic trigger and a $10 \times 10 \times 1$ cm striking plate. We removed 1–5 cm of the upper organic layers to ensure the best contact of the geophones and the steel plate with the ground. A 5 kg sledge hammer can produce about 150 Nm, which results in vertical blow energy valid for a depth range of 2–40 m in Quaternary sediments. Stacking three blows at each source point reduces background noise and increases the energy due to compression of the upper centimeters of the rather loose upper surface (Krummel, 2005). Calculated subsurface models were compared with GPR-data and with descriptions of drilling logs from adjacent borings.

Radar lines were collected using a portable RAMAC CU II GPR system (MALÅ Geosystems). We used 25, 100, and

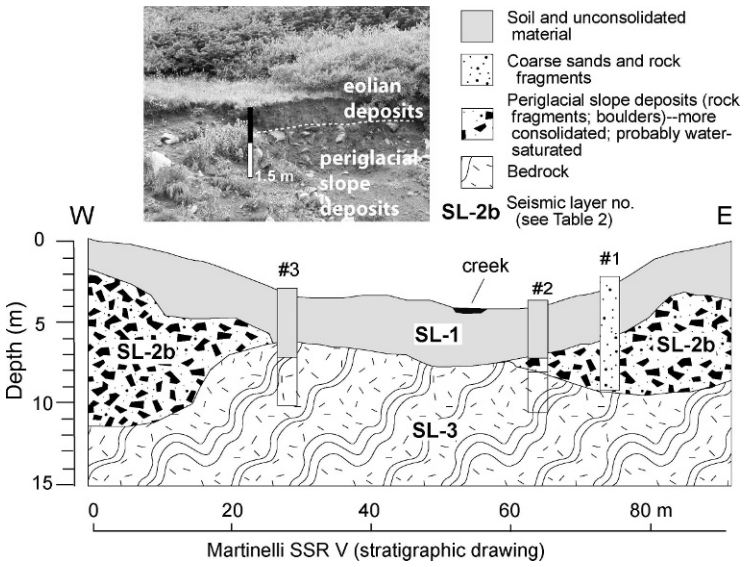

FIGURE 2. Final stratigraphic model for the Martinelli Snowfield site, showing materials, layering, and graphic logs from borings adjacent to the seismic line together with the numbers of seismic layers. Inset image shows a shallow subsurface section at a road cut 40 m downhill from the seismic line. Note that fine unconsolidated eolian material caps periglacial slope deposits. Calculated seismic velocities and their interpretation are listed in Tables A1 and A2 in Appendix A.

200 MHz antennae to obtain 2D-profiles. In this paper we present data collected with the 100 MHz antennae; this frequency consistently gave the best results. During the field survey the antennae were spaced 1 m apart, parallel to each other and perpendicular to the direction of the survey line. We collected data every 0.25 m and each trace of every line was stacked 16 times. Common midpoint surveys (CMP) were carried out in several areas to measure local electromagnetic wave velocity. Interpretation was based on visual inspection of the reflection pattern following Neal (2004), comparison to descriptions from nearby drill cores, SSR data, and data collected in previous studies.

Results

The 6 SSR and 13 GPR lines were collected over a total distance of 1465 m in the Niwot Ridge area. Here we present data from 5 SSR and 5 of the GPR lines from the south slopes of Niwot Ridge. Combined with previous field studies (e.g. Benedict, 1970; Ives and Fahey, 1971), results allow us to model the shallow subsurface at the study sites in considerable detail.

SHALLOW SEISMIC REFRACTION

The location, length, and physical settings of the survey lines in the Niwot Ridge area (Fig. 1a) were optimized to test the value of rapidly collected, non-invasive methods in studying the shallow subsurface. Stratigraphic images mainly were interpreted in terms of two main refractors and a three-layer model that suggests comparable stratigraphic sequences. Calculated velocities (Appendix A, Tables A1 and A2) are appropriate for the subsurface materials and bedrock (e.g. Hecht, 2003; Fertig, 2005; Burger et al., 2006). We briefly discuss here how we used seismic data to construct models of the critical zone below Martinelli Snowfield (Fig. 2) and at Niwot Trough (Fig. 3), sites located at treeline at 3430 m, above the late Pleistocene glacial limit. The Martinelli site slopes at about 14° whereas the Niwot Trough site has an 18° slope.

Seismic refraction data allow us to calculate preliminary, mainly three-layer models for all lines except the line Niwot SSR I where data provided a four-layer model. Velocities range from 233–368 m s^{-1} for the top layer (SL-1), followed by the first refractor with 567-777 m s^{-1} (SL-2a) at the Niwot Trough site

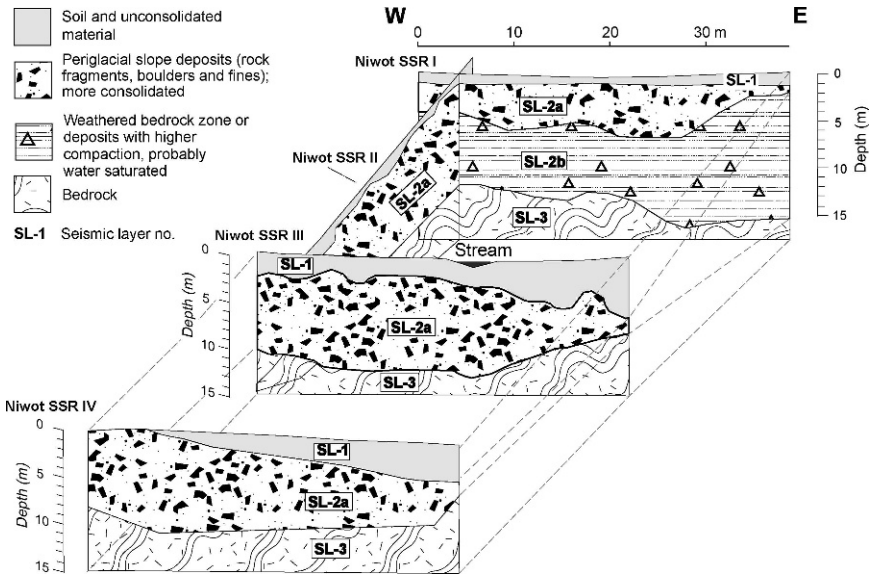

FIGURE 3. Fence diagram showing the stratigraphic model for lines Niwot I, II, III, and IV at the Niwot Trough site together with the numbers of seismic layers. Calculated seismic velocities and their interpretation are listed in Tables A1 and A2 in Appendix A.

and 1301 m s^{-1} (SL-2b) at Martinelli SSR V (Appendix A, Table A1). For Niwot SSR I we calculated a layer SL-2b with a velocity of 1650 m s^{-1}. Calculated velocity for the basal layer was between 2908 and 3920 m s^{-1} (SL-3) at Niwot SSR I–IV. At Martinelli SSR V, the third layer gives a velocity of 4400 m s^{-1} (SL-3). The calculated depth, dip, and thickness of the two subsurface refractors vary at the different study sites (Figs. 2 and 3). Near Martinelli Snowfield, layer one (SL-1) is 2–3 m thick, whereas modeled layer 2 (SL-2b) has a maximum thickness of 9 m and pinches out toward the center of the seismic line. The base of layer 2 (SL-2b) is 12 m below the surface on the west and 9 m on the east, and the model indicates considerable variation in thickness. Borehole #1 was logged as mixed sand and gravel, whereas materials and depths to bedrock in boreholes #2 and #3 correspond to the interpreted seismic results (Fig. 2).

At the Niwot Trough site, Niwot SSR lines II–IV give relatively simple solutions using a 3-layer model, whereas Niwot SSR I gives a best fit using 4 layers (Fig. 3). The top layer (SL-1) in all lines has a maximum thickness of 5 m and an average thickness of about 2.5 m. Layer two (SL-2a and SL-2b for Niwot SSR I) varies in thickness and reaches a maximum value of 13 m. The upper boundary of the basal layer (SL-3), which gives velocities typical of bedrock (see Appendix A), varies between 7 and 15 m below the surface and averages about 10 m. Layer contacts indicate erosion and deposition in an area where a modern seasonal stream has cut down 1–3 m into the deposits.

GROUND PENETRATING RADAR

The images derived from the GPR-survey at the East Knoll and the Fahey site (Fig. 1d) were produced using methods noted above and are displayed using a two way travel time (TWT) and a depth scale calculated using the velocities of Table 3 (see Appendix A).

Results from Common Midpoint (CMP) Surveys

Filtered measurements from the several CMP lines we collected show that subsurface velocity is variable (Tables A3 and A4 in Appendix A). CMP surveys can give information of the subsurface signal velocity (Fig. 4). Changes in signal velocity are a result that we interpret in terms of different material properties. On top of the West Saddle (Fig. 1a), for instance, we measured velocities of 0.09 m ns^{-1}, consistent with adjacent pit exposures of dry, coarse material with an openwork matrix (e.g. periglacial weathered blocks, see also Degenhardt et al., 2003). In contrast, at the Fahey site we calculated mean velocities of 0.078 m ns^{-1}, locally 0.055 m ns^{-1} (Fig. 4). The first velocity (0.078 m ns^{-1}) likely reflects material similar to that at the West Saddle, but wetter or richer in fines (clay and silt). We used this velocity for the time-depth conversion of the radar images at the Fahey site. The 0.055 m ns^{-1} velocity, which was measured beneath a solifluction lobe, is typical of water-saturated material containing abundant fines and possibly organic material (e.g. Davis and Annan, 1989; Moorman et al., 2003; Blindow et al., 2005). At both CMP lines at the Fahey site, the velocity of the electromagnetic waves increased sharply to a maximum of 0.12 m ns^{-1} at a depth of about 2.2 m. At FAH-CMP II (adjacent to a solifluction lobe) velocity decreased to 0.085 m ns^{-1} at a depth of 3.3 m (see Fig. 4a). At FAH-CMP I (on a solifluction lobe), the signal is attenuated with depth due to the high water content and the fine silty and organic rich material of the upper 2 m; interpretation of deeper signals is necessarily tentative. Drill core logs in the vicinity of the Fahey site show depth to bedrock >7.2 m (e.g. Fig. 6); high velocity at shallow depth cannot reflect bedrock.

East Knoll

At the East Knoll site (Fig. 1a), our survey sampled a dry, 11° slope with a 75 m line extending from a bedrock outcrop down across a mainly inactive blockfield. At the summit, an old prospecting pit exposes a fractured bedrock surface between 1 and 1.5 m below the land surface. GPR penetration depth extends a maximum of 200 ns or 9 m at a velocity of 0.09 m ns^{-1}. Our radar image (not shown in this paper), which was collected beginning 3 m from the center of the pit, was dominated by hyperbolic diffractions typical of subsurface boulders. Several subparallel reflections were present, mainly in the upper 20 m of the line. The reflection which dips at an apparent angle of about 14° disappears downslope.

Fahey Site

At the Fahey site we collected 5 GPR lines designed to sample a broad area and to include as many surface environments as possible near active or recently active periglacial lobes and seasonally ponded surface water (Fig. 1d). All GPR images are characterized by near-surface parallel to subparallel, laterally continuous reflections (Fig. 5). More hyperbolic features appear at greater depth, representing diffractions of the electromagnetic wave typically caused by a point source. The deepest penetration was about 200 ns (TWT) or 7.8 m using a velocity of 0.078 m ns^{-1}. In addition to characteristic and repeated reflection patterns, at Fahey 100 I between 7 and 20 m, an onlap reflection (at 150 ns) clearly extends over an oblique reflection. At Fahey 100 II, between 35 and 48 m, parallel reflections (at 220–270 ns) dominate the generally dipping survey line. On all surveys radar signals are attenuated along different parts of the lines (dotted line with double points in Fig. 5). Zones of attenuation are 2–3 m below the surface and vary in length from a few to more than 50 m. On some lines, signals from these areas are characterized by "ringing," most likely caused by an impedance mismatch between the transmitter and the receiver antenna with the ground (Radzevicius et al., 2000). Such ringing interferes to greater or lesser degrees with interpretation of the radar image at these positions.

Discussion

Geophysical data that were collected during late July 2005 allow an initial assessment of shallow subsurface layers and their continuity in the vicinity of Niwot Ridge. Our interpretations are the first from the area that combine results from GPR and SSR surveys to obtain subsurface information down to bedrock. Geophysical data and borings suggest that layered subsurface materials are >7 m thick in most areas of Niwot Ridge we studied and that ice lenses are present seasonally beneath active solifluction lobes but not in other areas. The data are site specific, but we discuss below how our results can be generalized and how they compare to previous studies in the area and in similar alpine zones.

SEISMIC DATA

Our model and drilling results portray unconsolidated material capped by soils (SL-1) and covering periglacial slope deposits consisting of layered rock fragments, boulders, and fines

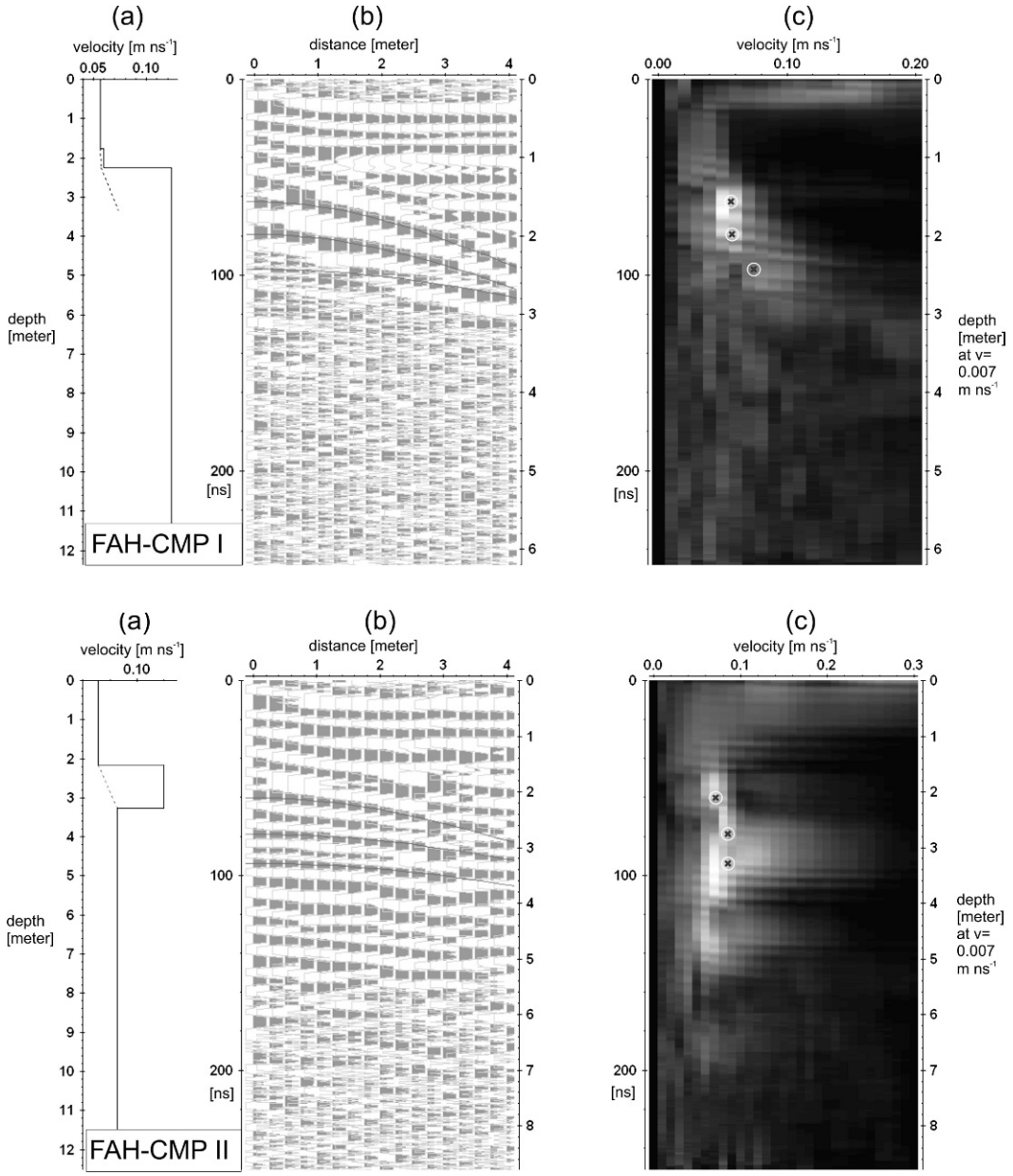

FIGURE 4. Velocity analysis of FAH-CMP I and FAH-CMP II lines. Subsurface velocity can be determined from CMP surveys which produce distance vs. travel time plots. Analysis of the hyperbola allows the calculation of subsurface velocity. (a) 1-D velocity model showing the calculated velocity (m ns^{-1}) with depth. (b) CMP solution showing linear dispersal of the ground wave from top left to upper right side and hyperbolic reflection events deeper in the section. (c) Semblance plot with picks of root-mean-square velocity marked with black crosses and white circles.

(e.g. SL-2a), which are slightly more consolidated than SL-1 (soils and unconsolidated material). At the Martinelli site, deposits of layer 2 have a slightly higher seismic velocity (SL-2b; 1301 m s^{-1}) than those at Niwot Trough (SL-2a; 567–777 m s^{-1}), suggesting consolidation by thick drifts of snow or that the material is partly water saturated. The rock fragments, boulders, and fines that comprise layer 2 at Martinelli are similar to drilling results, which describe water saturated coarse sands and gravels at depths similar to those of layer 2.

At all sites the basal layer (SL-3) is bedrock (Appendix A, Table A2), mapped as Precambrian gneiss or early Tertiary intrusive rocks (Gable and Madole, 1976). Boreholes at the Fahey site and adjacent to our lines at Martinelli indicate a variable stratigraphy of surficial deposits and suggests that local depth to bedrock mainly is >7 m.

We interpret the deepest layers at Niwot Trough and Martinelli as bedrock rather than permafrost, which could produce velocities of 3100–4500 m s^{-1} (Hecht, 2003). It is unlikely that the deepest layers represent permafrost. We would expect that the upper surface of frozen deposits would show relatively smooth, flat boundaries, something we did not observe in our seismic lines. The Martinelli drill holes provide general confirmation for our seismic interpretations and neither permafrost nor small ice lenses were detected during drilling two months after the late July SSR survey. GPR results from the Martinelli site also indicated that neither ice lenses nor permafrost were present (Leopold, unpublished data, 2005). Borehole #3 shows coarse sand and gravel (which we interpret as soils and unconsolidated material of SL-1) over bedrock at a depth of about 4.5 m, nearly identical to the seismic refraction model (SL-3). The calculated three-layer model

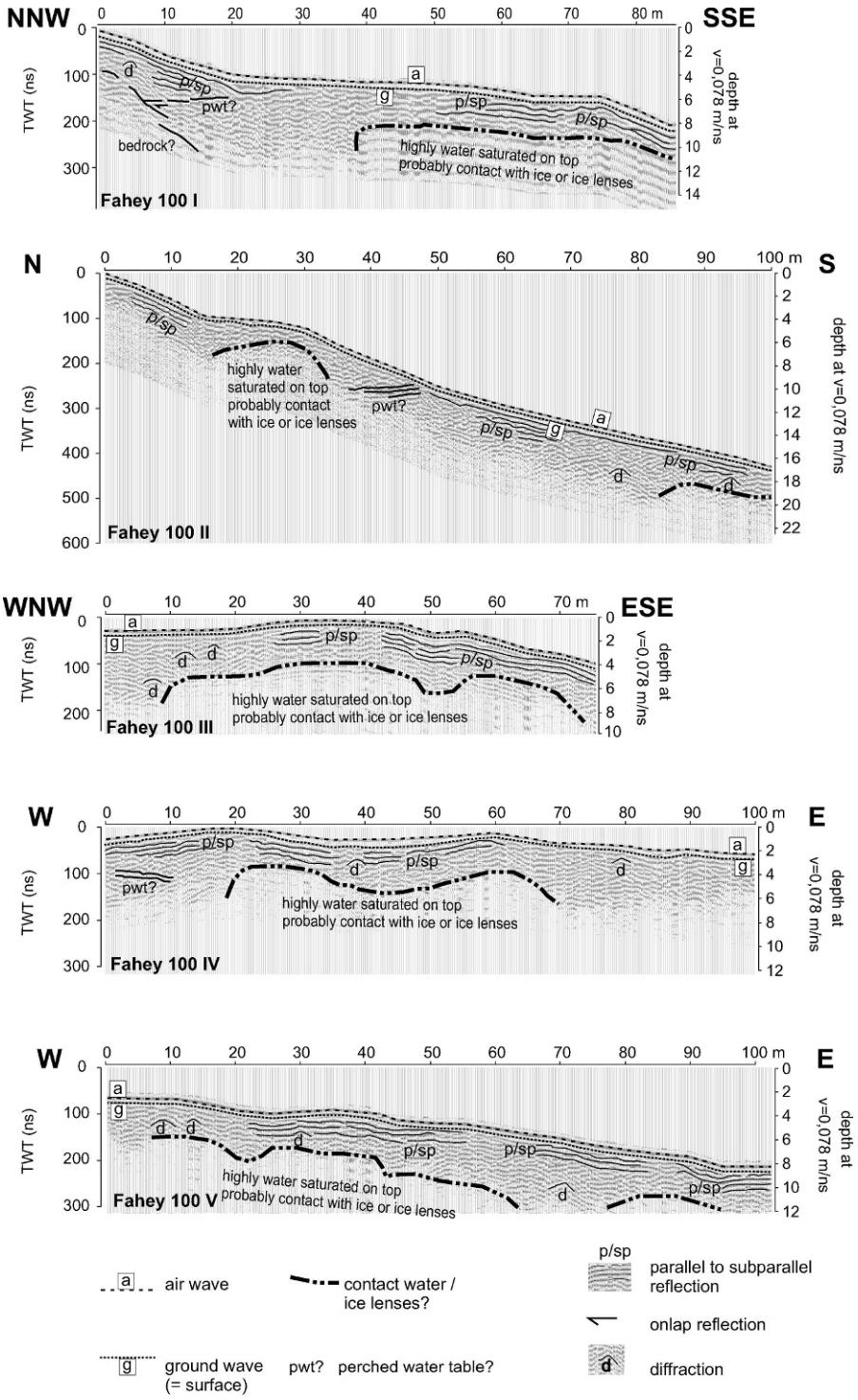

FIGURE 5. 100 MHz GPR lines of Fahey 100 I–V, showing two way travel-time (TWT) on the left axis, and a time to depth conversion on the right axis. The images are characterized by many hyperbolic diffractions (probably small boulders) and areas with reduced signal penetration noted with dashed lines and double points. Note parallel to subparallel reflections which are characteristic for sediments that have been transported down slope by periglacial processes.

at the approximate position of borehole #2 is also similar to the results of the drill core description. Drill core #1 shows coarse sands and gravels, no stratigraphic break, and depths to bedrock >8 m, but the hole was ~6 m from our line. Beside the offset of drill core #1 from the seismic refraction line, we note the difficulties in lithogenic description of subsurface material with the chosen drilling method. Nevertheless, relatively close correspondence in depth to bedrock and other subsurface strata description between drill core descriptions and seismic refraction models suggests the considerable potential of seismic refraction for detailed models of the shallow subsurface.

RADAR DATA

The shallow subsurface of the alpine environment at Niwot Ridge is most effectively portrayed using a frequency of 100 MHz, giving a penetration depth of 9 m in the dry upper slopes and 3 m at the wet, silt-rich sites. The GPR line at East Knoll was dominated by hyperbolic diffractions that result from point sources such as boulders (Jol and Bristow, 2003). Bedrock about 1.4 m below the surface at the east end of the line did not correspond to a reflection at this depth in the radar image. These results suggest that an angular and undulating bedrock surface

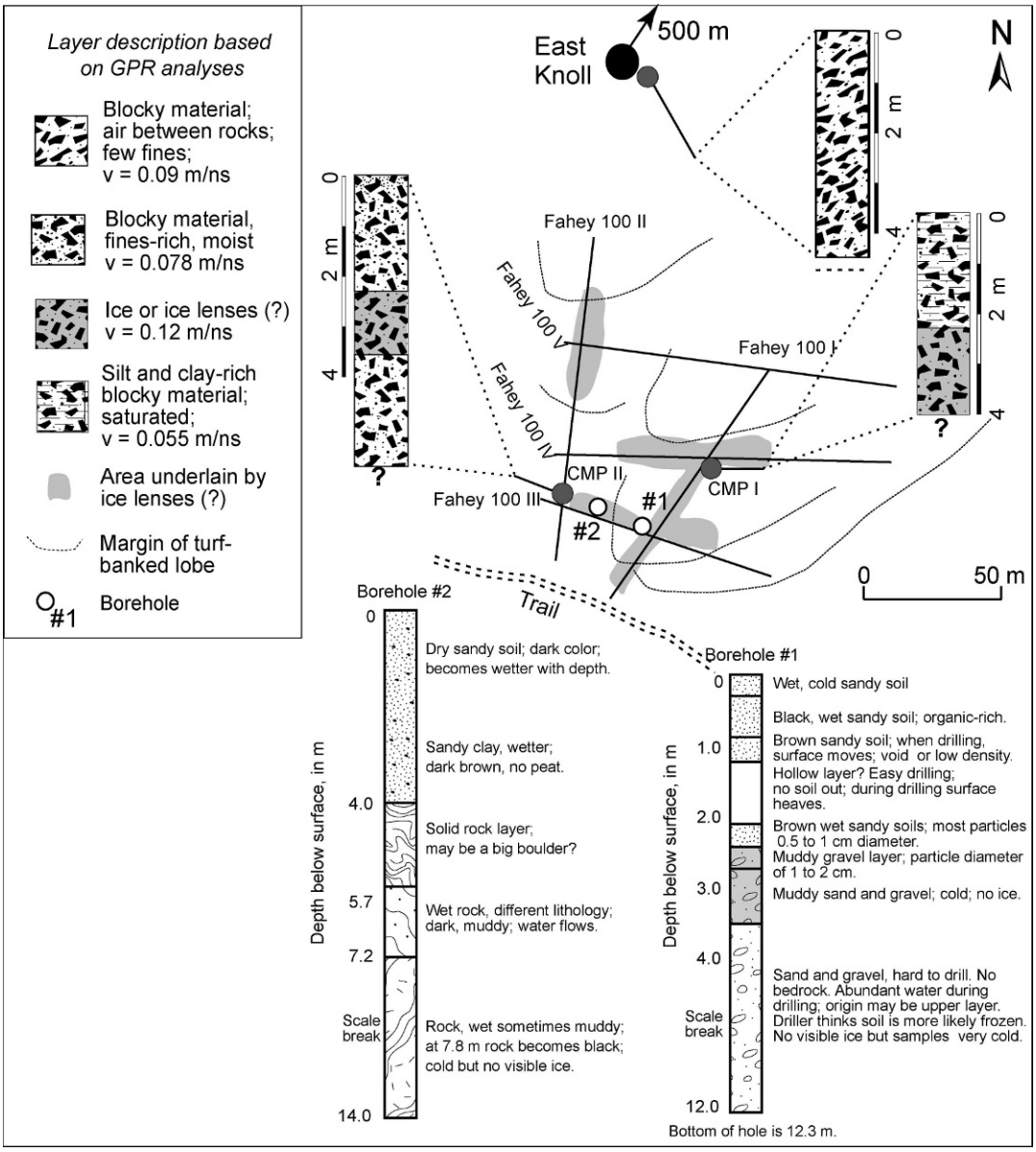

FIGURE 6. Sketch map of Fahey site showing the location of measured lines and the sites of CMP measurements together with the general distribution of the solifluction lobes. Gray shading highlights areas possibly underlain by ice lenses in the shallow subsurface. Profiles and the layer descriptions are derived from GPR images and velocity analysis. Grayish black circles show the location of CMP survey. CMP I is on the solifluction lobe, whereas CMP II is on the dry area west of the lobe. Open bullets show location of two boreholes, one on the solifluction lobe and the other at the edge of the lobe. Generalized lithogenic sketches and descriptions (modified from field log of Tingjun Zhang) interpreted from borings. Holes were drilled two months after the GPR survey using an air compressor technique which allows only general description of the lithogenic subsurface material (K. Chowanski, INSTAAR, personal communication, 2006).

acts as a single point source and causes diffraction signals. The oblique and continuous reflection that we observed at a depth of 3–3.5 m on the top of the hill deepens to >6 m downslope and probably represents less fractured bedrock. The GPR lines Fahey 100 I–V also display numerous hyperbolic diffractions (Fig. 5). Continuous horizontal lines probably represent the local water table at Fahey 100 I and II. These reflections are dominant, truncate other reflections and are partly characterized by two or more reflections. At Fahey 100 I, the saturated surface interpretation is consistent with the small ponds in low areas of the lobe and with a small stream that drains the area.

The GPR data and field observations highlight a suite of subsurface hydrologic features noted with dashes and double points in Figure 5. These features are sharply zoned in the radar image where the signal is attenuated with depth and identified in Figure 6 with a gray color. Radar penetration on the margins of these areas is greater than in their centers. FAH-CMP I and FAH-CMP II were collected across a discontinuity in the subsurface next to a solifluction lobe (see Fig. 6). The slow velocity (0.055 m ns^{-1}) of the upper 2 m of the lobe is probably a result of high water content and abundant fines (silts). Benedict (1970) described the upper 2 m of lobe '45' as a poorly sorted silt loam with blocky structure and high soil moisture content.

Below the wet, fine-grained sediment, a sharp increase in velocity to 0.12 m ns^{-1} at a depth of about 2.2 m suggests the presence of ice lenses. Ice gives GPR velocity values of 0.106–0.16 m ns^{-1}, depending on the degree of saturation (Davis and Annan, 1989; Degenhardt et al., 2003; Moorman et al., 2003; Blindow et al., 2005). Dry coarse sands or bedrock can give similar velocities, but there is no evidence for these materials here. The

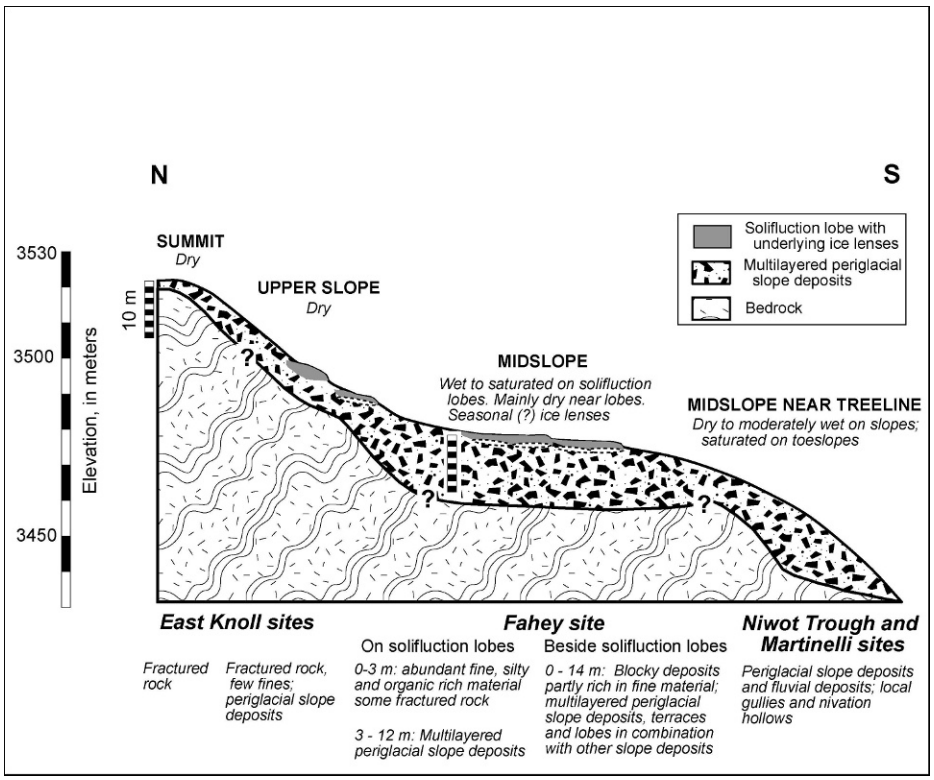

FIGURE 7. Schematic cross section at Niwot Ridge portraying the composition of the shallow subsurface, lateral thickness variation, and local variation in moisture and ice content over a downslope distance of approximately 800 m. Vertical exaggeration is approximately four times. The image summarizes data acquired by our SSR and GPR studies, modified by data from drill cores, outcrops, and previous studies.

local high velocities suggest that ice or ice lenses were present when we sampled within the solifluction lobes and at isolated sites outside lobes. Ives and Fahey (1971, p. 108) described ice lenses and layers, at the end of August, 1.9 m below the surface of a lobe 50 m downslope from our site. They also suggested that extensive areas of permafrost with an active layer <2 m thick may persist under wet sites at altitudes between 3750 and 3800 m on Niwot Ridge (Ives and Fahey, 1971: 109). We found no indication of deeper ice lenses or frozen ground in dry areas at sites below an elevation of about 3550 m.

Strong attenuation of the GPR signal suggests that ice inferred from our measurements probably is mixed with water at the contact zone; a water-rich interface may account for ringing signals below the contact zone. The shape of the inferred ice surface is uneven, presumably reflecting uneven distribution of ice lenses and nonuniform freezing and thawing. Higher velocity at CMP II, which represents the dry sites west of the solifluction lobe, is restricted to a layer of about 1 m thickness. If the layer is ice or ice-rich fine sediment, its low permeability and hydrologic focusing may explain local areas of seasonally ponded water on the solifluction lobe. The drill core descriptions at the Fahey site generally confirm the sediment properties interpreted from GPR (see Fig. 6) but again we point out the difficulties in lithogenic description of the subsurface material using the drilling method. Although drilling did not detect ice 2 months after our survey in late July 2005, zones in the drill cores described as hollow layers might represent uncollapsed voids left after ice lenses melted (Fig. 6) and the cold temperatures could reflect frozen zones of sediment.

Perhaps the permafrost modeled by Ives and Fahey has degraded in the past 35 years (e.g. Janke, 2005). However, with the possible exception of a local zone under a small hill at Fahey 100 II (15–32 m), in the 460 m of GPR lines we ran in the Fahey area, we only found seasonal ice lenses and highly water saturated material beneath turf-banked lobes and adjacent areas. Benedict (1970) used measurements of groundwater levels to illustrate how seasonal fluctuations of water-table height and shrinking and swelling of the saturated area were related to movement of the turf-banked lobe at site 45. GPR measurements and topographic relations provide a rapid means of surveying such areas, which probably represent the most active geomorphic, hydrologic, and biologic zones within the alpine environment at Niwot Ridge.

Implications for Geomorphic Studies on Niwot Ridge and in Other Sensitive Alpine Zones

Geophysical methods provide efficient, non-invasive tools for mapping and visualizing the critical zone in environmentally sensitive areas. The combined application of SSR and GPR provides data about depth to bedrock and stratigraphic relations and allows inferences about hydrological and physical properties of the shallow subsurface in a 2D-framework. Normally such information is collected in one dimension using soil pits or augering, which can limit the explanatory power of models based on simple linear extrapolation. Detailed understanding of subsurface variation provides tools essential for geomorphic, hydrologic, and pedological studies. Based on this study and other geophysical lines we have run in nearby alpine areas, drilling information, and previous work, we present a schematic cross section (Fig. 7) running from the summit of Niwot Ridge down to tree line at about 3450 m a.s.l.

Figure 7 indicates that the subsurface stratigraphy is variable in depth to bedrock (1 to >14 m) and in stratigraphic layering and composition (coarse, angular boulders to organic-rich fine sediments). Water content and inferred subsurface drainage varies spatially and seasonally as snowdrifts melt. Regolith models (e.g. Heimsath et al., 1997) and other geomorphic studies examine linear and non-linear control of regolith thickness by slope distance and angle. Seastedt et al. (2004) noted that gelisolifluction and frost creep are major factors in explaining site-

to-site differences in ecologically based studies, which influences their landscape continuum model. Figure 7 allows us to make basic geomorphic observations about periglacial deposits from the ridge crest downhill across a carefully studied area.

Regolith rich in periglacial deposits covers the area from the ridge crest downslope, thickening to at least 12 m locally on the midslope bench at the Fahey site and thinning downslope toward the glaciated valley. Thickness of regolith is not simply related to slope on this transect. At 500 m from the summit at the bench, the Fahey site has an average regolith thickness of 9 $\pm$ 2.5 m. At a distance of 700–800 m, the slope steepens, shallow gullies are present, and average thickness is 8 $\pm$ 5.25 m. In areas away from the East Knoll summit we measured variable regolith thickness that did not seem to depend on local slope. Other factors, most notably water availability and the frequency of heaving cycles, are more significant than slope angle for local solifluction processes. Local slope also may be different than paleoslope, which could have been greater. Periglacial processes likely smoothed the slopes of a now-buried landscape, as is the case in other places (e.g. Kleber, 1997; Völkel et al., 2001).

The considerable thickness of the critical zone is a striking feature of this part of Niwot Ridge, where bedrock is not exposed in the alpine zone except on the steepest local slopes and in a few summit areas. Our profile suggests that periglacial processes have removed regolith from the steep slopes of the East Knoll but have not stripped the weathered mantle in most areas. Benedict (1970) mapped different generations, rates of advance, and fossilization times for solifluction lobes and terraces in the nearby area. He noted that lobe motion is episodic and depends mainly on local moisture conditions. Reconstructed motion was relatively slow during Holocene time, but faster during the latest Pleistocene. Our field observations noted multi-layered slope deposits at a road cut close to the Martinelli snowfield, and several descriptions from drilling (see Fig. 6) and data from seismic refraction (Fig. 3) and high-resolution GPR images suggest layered deposits are typical of the shallow subsurface. Generations of lobes are also known from the European Alps and the European mid hills (e.g. Veit, 1993; Völkel and Leopold, 2001).

Our measurements and previous studies in the Niwot Ridge area show that the relatively thick deposits underlying the midslope bench provide seasonal water storage and discharge points for shallow ground-water systems (Fig. 6). In this area local ponds and little streams demonstrate seasonal saturation, possibly caused by ice lenses beneath solifluction lobes (e.g. Fig. 6; Benedict, 1970). Drilling data document water in the vicinity of the solifluction lobes, GPR velocity analysis denotes water-saturated fine sediments on top of the lobes, and GPR reflections (Fig. 5) show the location of near-surface water tables at these sites. Various authors show that there is a close connection between shallow subsurface water and the rate of regolith transport. Local surface topography does not appear to concentrate subsurface flow directly, but snow accumulation patterns, permeability characteristics of the layers in the shallow subsurface, and the shape of the buried bedrock surface may also be important. At other slope positions we have noted slight velocity variations in the SSR survey, which might indicate different amounts of interstitial water.

The results described document the physical and local hydrologic properties of slope deposits in some areas of Niwot Ridge. Geomorphic and biogeochemical studies need to account for the layering and variability of these slope-forming materials, which can be studied using geophysical methods. The geophysical techniques described here require walking across the ground carrying instruments (GPR) and digging a few 10 $\times$ 10 $\times$ 5 cm holes for the seismic lines; negative effects on vegetation or other research are minimal, which makes the methods valuable for research in sensitive areas. Under ideal conditions, near-3D coverage is possible using closely spaced lines, but field collection of data and processing time increase exponentially. Measurements can also be repeated over time where measuring a time series can be used to define changing conditions, e.g. the status of subsurface permafrost or the control of water availability.

Acknowledgments

We wish to thank the Deutsche Forschungsgemeinschaft (DFG-Az. Leopold USA 444 USA 111/8/05) and the Sperry Research Fund (Williams College), which helped to fund this research. The studies were partly carried out under the funding framework of "Boulder Creek Critical Zone Observatory (CZO)" sponsored by the U.S. National Science Foundation (NSF) proposal 0724960. The studies were done in cooperation with the Mountain Research Station (MRS) of the University of Colorado at Boulder, U.S.A., which we thank for logistical help. Thanks to Dr. Peter Birkeland and Dr. Jim Benedict for their help in the field and useful discussions. We also thank Kurt Chowanski from the Institute of Arctic and Alpine Research (INSTAAR) for providing the drill core data. Logistical support and/or data were provided by the NSF–supported Niwot Ridge Long Term Ecological Research project and the MRS. We also want to thank two anonymous reviewers and the associate editor for their comments and their constructive improvements made to the paper.

References Cited

Anderson, S. P., von Blankenburg, F., and White, A. F., 2007: Mechanical-chemical interactions shape the Critical Zone and fluxes from it. *Elements*, 3: 315–319.

Barry, R. G., 1973: A climatological transect on the east slope of the Front Range, Colorado. *Arctic and Alpine Research*, 5: 89–110.

Benedict, J. B., 1970: Downslope soil movement in a Colorado alpine region: rates, processes, and climatic significance. *Arctic and Alpine Research*, 2: 165–226.

Benn, D. I., and Evans, D. J. A., 1998: *Glaciers and glaciations*. London: Arnold, 734 pp.

Berthling, I., Etzelmüller, B., Wåle, M., and Ludvig, V. J., 2003: Use of Ground Penetrating Radar (GPR) soundings for investigating internal structures in rock glaciers. Examples from Prins Karls Forland, Svalbard. *In* Schrott, L., Hördt, A., and Dikau, R. (eds.), *Geophysical Applications in Geomorphology. Zeitschift für Geomorphologie, N.F. Supplement*, 132: 103–121.

Birkeland, P. W., Shroba, R. R., Burns, S. F., Price, A. B., and Tonkin, P. J., 2003: Intergrading soils and geomorphology in mountains—An example from the Front Range of Colorado. *Geomorphology*, 55: 329–344.

Blindow, N., Richter, T., and Petzold, H., 2005: Bodenradar. *In* Knödel, K., Krummel, H., and Lange, G. (eds.), *Geophysik. Handbuch zur Erkundung des Untergrundes von Deponien*, 3: 389–424.

Burger, H. R., Sheehan, A. F., and Craig, J. H., 2006: *Introduction to applied geophysics: exploring the shallow subsurface*. New York: Norton & Company, 554 pp, with appendix.

Davis, J. L., and Annan, A. P., 1989: Ground Penetrating Radar for high resolution mapping of soil and rock stratigraphy. *Geophysical Prospecting*, 37: 531–551.

Degenhardt, J. J., Giardino, J. R., and Junk, B. M., 2003: GPR survey of a lobate rock glacier in Yankee Boy Basin, Colorado, USA. *In* Bristow, C. S., and Jol, H. M. (eds.), *Ground Penetrating Radar in Sediments.* Geological Society, London, Special Publication, 211: 167–179.

Fertig, J., 2005: Seismik—Prinzip der Methode. *In* Knödel, K., Krummel, H., and Lange, G. (eds.), *Handbuch zur Erkundung des Untergrundes von Deponien*, 3: 425–466.
Gable, D. J., and Madole, R. F., 1976: Geologic map of the Ward Quadrangle, Boulder County, Colorado. U.S. Geological Survey Geologic Quadrangle Map GQ-1277, scale 1:24,000.
Greenland, D., 1989: The climate of Niwot Ridge, Front Range, Colorado. *Arctic and Alpine Research*, 21: 380–391.
Hambrey, M. J., 1994: *Glacial environments*. London: UCL Press, 296 pp.
Hecht, S., 2003: Differentiation of loose sediments with seismic refraction methods—Potentials and limitations derived from case studies. *In* Schrott, L., Hördt, A., and Dikau, R. (eds.), *Geophysical Applications in Geomorphology. Zeitschift für Geomorphologie, N.F. Supplement*, 132: 89–102.
Heimsath, A. M., Dietrich, W. E., Nishiizumi, K., and Finkel, R. C., 1997: The soil production function and landscape equilibrium. *Nature*, 388: 358–361.
Hoffmann, T., and Schrott, L., 2003: Determining sediment thickness of talus slopes and valley fill deposits using seismic refraction—A comparison of 2D interpretation tools. *In* Schrott, L., Hördt, A., and Dikau, R. (eds.), *Geophysical Applications in Geomorphology. Zeitschift für Geomorphologie, N.F. Supplement*, 132: 71–87.
Ives, J. D., and Fahey, B. D., 1971: Permafrost occurrence in the Front Range, Colorado Rocky Mountains, U.S.A. *Journal of Glaciology*, 10/58: 105–111.
Janke, J. R., 2005: The occurrence of alpine permafrost in the Front Range of Colorado. *Geomorphology*, 67(3–4): 375–389.
Jol, H. M., and Bristow, C. S., 2003: GPR in sediments: a good practice guide. *In* Bristow, C. S., and Jol, H. M. (eds.), *Ground Penetrating Radar in Sediments.* Geological Society, London, Special Publication, 211: 9–27.
Kirsch, R., and Rabbel, W., 1997: Seismische Verfahren in der Umweltgeophysik. *In* Beblo, M. (ed.), *Umweltgeophysik*. Berlin: Ernst & Sohn, 243–311.
Kleber, A., 1997: Cover-beds as soil parent materials in mid-latitude regions. *Catena*, 30: 197–213.
Krummel, H., 2005: Seismische Quellen. *In* Knödel, K., Krummel, H., and Lange, G. (eds.), *Handbuch zur Erkundung des Untergrundes von Deponien und Altlasten*, 3: 467–504.
Leopold, M., and Völkel, J., 2003: Radar images of periglacial slope deposits beneath peat bogs in Middle European Highlands, Germany. *In* Bristow, C. S., and Jol, H. M. (eds.), *Ground Penetrating Radar in Sediments.* Geological Society, London, Special Publication, 211: 177–185.
Leopold, M., and Völkel, J., 2007a: Colluvium: definition, differentiation and possible suitability for reconstructing Holocene climate data. *Quaternary International*, 162–163: 133–140.
Leopold, M., and Völkel, J., 2007b: Quantifying prehistoric soil erosion—The discussion of different methods by the example of a Celtic square enclosure in southern Germany. *Geoarchaeology*, 22[8]: 873–889.
Leopold, M., Völkel, J., and Heine, K., 2006: A ground penetrating radar survey of late Holocene fluvial sediments in northwest Namibian river valleys: characterisation and comparison. *Journal of the Geological Society*, 163: 923–936.
Madole, R. F., 1982: Possible origins of till-like deposits near the summit of the Front Range in north-central Colorado. U.S. Geological Survey Professional Paper 1243, 31 pp.
Menzies, J., 1996: *Past glacial environments: sediments, forms and techniques*. Oxford: Butterworth-Heinemann, 598 pp.
Moorman, B., Robinson, S., and Burgess, M., 2003: Imaging periglacial conditions with ground penetrating radar. *Permafrost and Periglacial Processes*, 14: 319–329.
Munroe, J. S., Doolittle, J. A., Kanevskiy, M. Z., Hinkel, K. M., Nelson, F. E., Jones, B. M., Shur, Y., and Kimble, J. M., 2007: Application of Ground-Penetrating Radar imagery for three-dimensional visualisation of near-surface structures in ice-rich permafrost, Barrow, Alaska. *Permafrost and Periglacial Processes*, 18: 309–321.
Neal, A., 2004: Ground-penetrating radar and its use in sedimentology: principles, problems and progress. *Earth-Science Reviews*, 66: 261–330.
Otto, J. C., and Sass, O., 2006: Comparing geophysical methods for talus slope investigations in the Turtmann valley (Swiss Alps). *Geomorphology*, 76: 257–272.
Raab, T., and Völkel, J., 2003: Late Pleistocene glaciation of the Kleiner Arbersee area in the Bavarian Forest, south Germany. *Quaternary Science Reviews*, 22: 581–593.
Raab, T., Völkel, J., and Leopold, M., 2007: Character, age, and ecological significance of Pleistocene periglacial slope deposits in Germany. *Physical Geography*, 28(4): 1–23.
Radzevicius, S., Guy, E., and Daniels, J., 2000: Pitfalls in GPR data interpretation: differentiating stratigraphy and buried objects from periodic antenna and target effects. *Geophysical Research Letters*, 27(20): 3393–3369.
Sandmeier, K., 2004: *Reflexw manual ver. 3.5*. Karlsruhe: Sandmeier Scientific Software, 377 pp.
Sandmeier, K., and Liebhard, G., 1997: Refraktionsseismik: Iterative Interpretationsmethoden. *In* Knödel, K., Krummel, H., and Lange, G. (eds.), *Handbuch zur Erkundung des Untergrundes von Deponien und Altlasten*, 3: 546–552.
Sass, O., and Wollny, K., 2001: Investigations regarding alpine talus slopes using ground penetrating radar (GPR) in the Bavarian Alps, Germany. *Earth Surface Processes and Landforms*, 26(10): 1071–1086.
Seastedt, T. R., Bowman, W. D., Cine, N., McKnight, D., Townsend, A., and Williams, M. A., 2004: The landscape continuum: a model for high elevation ecosystems. *BioScience*, 54/2: 111–121.
Sheriff, R. E., and Geldart, L. P., 1982: *Exploration Seismology. Volume 1: History, Theory and Data Acquisition*. New York: Cambridge University Press, 272 pp.
Veit, H., 1993: Holocene solifluction in the Austrian and southern Tyrolean Alps: dating and climatic implications. *Paläoklimaforschung*, 11: 23–32.
Völkel, J., and Leopold, M., 2001: Zur zeitlichen Einordnung der jüngsten periglazialen Aktivitätsphase im Hangrelief zentraleuropäischer Mittelgebirge. *Zeitschrift für Geomorphologie,* N.F., 45/3: 273–294.
Völkel, J., Leopold, M., and Roberts, M. C., 2001: The radar signatures and age of periglacial slope deposits in the Central European Highlands of Germany. *Permafrost and Periglacial Processes*, 12: 379–387.

Ms accepted February 2008

Appendix

PROCESSING METHODS AND TABLES SUMMARIZING RESULTS OF SHALLOW SEISMIC REFRACTION (SSR) AND GROUND PENETRATING RADAR (GPR) DATA, NIWOT RIDGE AREA, COLORADO

For SSR, we used ReflexW 3.5.7 (Sandmeier Software; Sandmeier, 2004) to calculate travel times and to develop a subsurface p-wave velocity model using the wavefront-inversion modeling method, which uses wave front construction to locate points on refracting surfaces, together with network-raytracing (Kirsch and Rabbel, 1997; Sandmeier, 2004). Network-raytracing calculates synthetic travel times and allows iterative modification of initial conditions to provide an optimal match of synthetic and measured travel times. According to Sandmeier and Liebhard (1997) model calibration is sufficient when total time difference is <2 ms (compare Table A1). After combining wavefront-inversion

and network-raytracing to generate a range of subsurface models and travel times, we iteratively adjusted initial conditions and seismic velocities to give the closest fit to measured travel times for the model layers at the Niwot Trough and Martinelli Snowfield sites (Table A2).

ReflexW 3.5.7 (Sandmeier Software; Sandmeier, 2004) was used for GPR data transformation and visualization. Several filtering steps were applied on each line (Table A3). The radar images are displayed in a "wiggle" mode. Depending on the zoom size the wiggles have been clipped and displayed with a changing multiplication factor (plot scale). Table A4 gives an overview of the several lines, their length, number of traces per meter, and the velocity that has been chosen to display the data.

TABLE A1

Summary of field settings and calculated values for shallow seismic refraction (SSR) lines collected in the vicinity of Niwot Ridge. The total calculated time difference measures the average between measured and calculated travel time for each line, based on the network-raytracing method.

Line	Length (m)	Geophone spacing (m)	No. of identified layers	Velocities layer 1 (m s^{-1})	Velocities layer 2a (m s^{-1})	Velocities layer 2b (m s^{-1})	Velocity layer 3 (m s^{-1})	Total time difference (ms)
Niwot SSR I	39	3	4	233	741	1650	3920	1.9
Niwot SSR II	39	3	3	234	707	—	3103	1.3
Niwot SSR III	39	3	3	284	777	—	2908	1.9
Niwot SSR IV	39	3	3	302	567	—	3388	1.4
Martinelli SSR V	91	7	3	368	—	1301	4399	1.4

TABLE A2

Overview of different layers (seismic layer = SL) interpreted from SSR models for sites at Niwot Ridge and near Martinelli Snowfield. For each modeled layer the velocity range and interpretation are noted as well as the depth to bedrock, which here is the seismic layer SL-3.

		Niwot Ridge				Martinelli	
Layer no.	Velocity (m s^{-1})	Interpretation	Bedrock depth (m)	Layer no.	Velocity (m s^{-1})	Interpretation	Bedrock depth (m)
SL-1	233–368	soil and unconsolidated material	—	SL-1	368	soil and unconsolidated material	—
SL-2a	567–777	periglacial slope deposits (rock fragments, boulders, and fines) slightly more consolidated than layer 1	—	—	—	—	—
SL-2b	1650	weathered bedrock zone or deposits with higher compaction (e.g. periglacial slope deposits, rocks, boulders, probably water saturated	—	SL-2b	1301	periglacial slope deposits (rock fragments, boulders,) more consolidated and probably water saturated	—
SL-3	2908–3920	crystalline bedrock	5–15	SL-3	4399	crystalline bedrock	3–12

TABLE A3

Sequence of processing steps applied to each ground penetrating radar (GPR) line using the software ReflexW.

Filter (name)	Filter description
import	import of the raw data into ReflexW
subtract mean dewow	1D-filter (running mean value was calculated for each value of each trace over a period of 10 ns and subtracted from the central point to eliminate a low frequency part)
time zero	sets the arrival of the airwave to zero at the graphical output
running average	2D-filter (a running average over a selectable number of traces (2) for each time step was performed to suppress trace-dependent noise)
background removal	2D-filter (a subtraction of an averaged trace which is built up from the chosen time/distance range of the actual section was applied below the ground wave to reduce background noise due to slight ringing in the antennae)
time cut-off	the displayed time range is set to a reasonable value
static correction	the topography of the survey lines is applied by a static shift of the start time of the several traces according to break of slopes using relief data

TABLE A4

Summary of field settings and calculated values for ground penetrating radar (GPR) lines collected in the vicinity of Niwot Ridge (Fig. 1d).

Line	Length (m)	Antennae (MHz)	No. traces m^{-1}	Velocity top 2 m (m ns^{-1})
Fahey 100 I	85	100	4	0.078
Fahey 100 II	100	100	4	0.078
Fahey 100 III	75	100	4	0.078
Fahey 100 IV	100	100	4	0.078
Fahey 100 V	105	100	4	0.078
East Knoll 100 I (not shown in this paper)	70	100	4	0.09